

# Mode-Center Placement of Monolayer WS<sub>2</sub> in a Photonic Polymer Waveguide

Angelina Frank,\* Justin Zhou,\* James A. Grieve, Ivan Verzhbitskiy, José Viana-Gomes, Leyi Loh, Michael Schmid, Kenji Watanabe, Takashi Taniguchi, Goki Eda,\* and Alexander Ling

The effective integration of 2D materials such as monolayer transition metal dichalcogenides (TMDs) into photonic waveguides and integrated circuits is being intensely pursued due to these materials' strong exciton-based optical response. This work presents a platform where a 2D heterostructure (WS<sub>2</sub>-hBN) is directly integrated into the photonic mode-center of a novel polymer ridge waveguide. Finite-difference time-domain simulations and collection of photoluminescence from the guided mode indicate that this system exhibits significantly improved waveguide-emitter coupling and mode confinement over a previous elastomer platform. This is facilitated by the platform's enhanced refractive-index contrast and a new method for mode-center integration of the coupled TMD. The integration is based on a simple dry-transfer process that is applicable to other 2D materials, and the platform's elastomeric nature is a natural fit to explore strain-tunable hybrid-photonic devices. The demonstrated ability of coupling photoluminescence to a polymer waveguide opens up new possibilities for hybrid-photonic systems in a variety of contexts.

optical properties in both linear and non-linear regimes.<sup>[1–4]</sup> They have also been shown to be capable of hosting single-photon emitters.<sup>[5–7]</sup> Besides the tunability of their bandgap in response to electric fields,<sup>[8,9]</sup> TMDs' exciton dynamics can be further modified through stacking into van der Waals heterostructures,<sup>[10]</sup> chemical doping,<sup>[11]</sup> and application of mechanical strain.<sup>[12]</sup> These properties are of particular interest in the context of Photonic integrated circuits (PICs) where the goal is to couple a photon-routing structure to elements with strong and tunable optical response.<sup>[13]</sup> Such circuits find applications in optical communication,<sup>[14]</sup> computation,<sup>[15]</sup> and sensing.<sup>[16–18]</sup> Integration of TMDs into photonic waveguides can be readily achieved by direct transfer, taking advantage of the material's van der Waals bonding nature.<sup>[19,20]</sup> To date,

## 1. Introduction

Monolayer transition metal dichalcogenides (TMDs) are a material class of great interest due to their exciton-based

most hybrid systems with an optically coupled 2D material realize placement away from the photonic mode's maximum (off-center placement) or at a dielectric interface, for example, close to an exposed fiber core,<sup>[21,22]</sup> at the end-face

A. Frank, J. A. Grieve, A. Ling  
Centre for Quantum Technologies  
National University of Singapore  
3 Science Drive 2, Singapore 117543, Singapore  
E-mail: angelina.frank@u.nus.edu

J. Zhou, I. Verzhbitskiy, L. Loh, G. Eda, A. Ling  
Department of Physics  
National University of Singapore  
2 Science Drive 3, Singapore 117551, Singapore  
E-mail: justinzhou@u.nus.edu; g.eda@nus.edu.sg

J. A. Grieve  
Quantum Research Centre  
Technology Innovation Institute  
Abu Dhabi, UAE

J. Viana-Gomes  
Departamento de Física  
Centro de Física  
Campus de Gualtar, Braga PT-4710 - 057, Portugal


M. Schmid  
4th Physics Institute and Research Center SCoPE  
University of Stuttgart  
Pfaffenwaldring 57, 70569 Stuttgart, Germany

K. Watanabe  
Research Centre for Functional Materials  
National Institute for Materials Science  
1-1 Namiki Tsukuba, Ibaraki 305-0044, Japan

T. Taniguchi  
International Centre for Materials Nanoarchitectonics  
National Institute for Materials Science  
1-1 Namiki Tsukuba, Ibaraki 305-0044, Japan

G. Eda  
Centre for Advanced 2D Materials  
National University of Singapore  
6 Science Drive 2, Singapore 117546, Singapore

G. Eda  
Department of Chemistry  
National University of Singapore  
3 Science Drive 3, Singapore 117543, Singapore

 The ORCID identification number(s) for the author(s) of this article can be found under <https://doi.org/10.1002/adom.202101684>.

DOI: 10.1002/adom.202101684

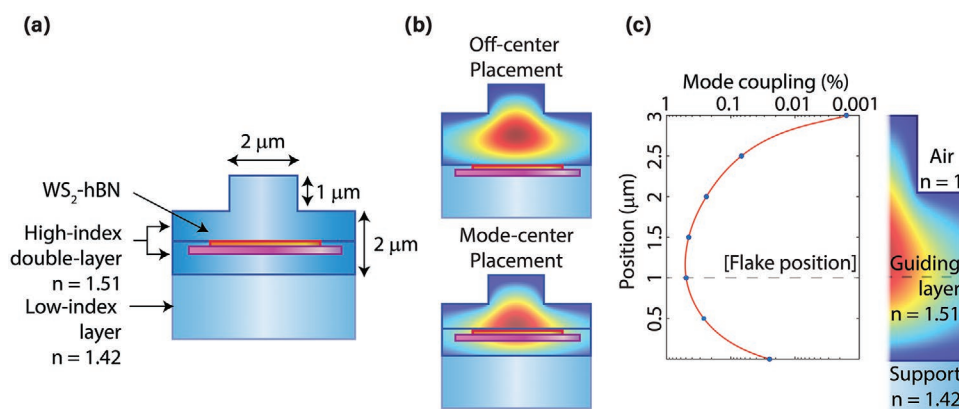


**Figure 1.** a) Schematic depiction of the waveguide with the integrated WS<sub>2</sub>-hBN heterostructure (thickness  $\approx 20$  nm). b) Illustration of off- and mode-center placement (emitter not drawn to scale) together with the mode profile. c) Simulation of a dipole source's emission at 620 nm coupling to the waveguide's fundamental mode for different vertical positioning. A maximum mode coupling of 0.49% in one propagation direction is predicted. The red line is intended as a guide to the eye.

of an optical fiber,<sup>[23]</sup> or on top of a waveguide in integrated photonic devices.<sup>[24–28]</sup>

As a proof of concept, we have previously demonstrated the integration of a TMD into an elastomeric ridge waveguide.<sup>[29]</sup> However, the optical coupling efficiency in this system is limited by the material's off-center placement in between high- and low-refractive index layers and a relatively low index contrast ( $n_1 - n_2 \approx 0.001$ ). A low index contrast also impedes mode confinement, limiting the performance of waveguide bends required, for example, for on-chip interferometers and more complex photonic circuits. Addressing these shortcomings opens up new applications for elastomeric waveguides. These hold particular promise for hybrid photonic systems, as their rapid, low-cost fabrication cycle provides a mild environment favoring the integration of various micro- and nano-structures. Potential applications include among others rapid-prototyping, foundational material studies and lab-on-a-chip systems.<sup>[30–34]</sup> An additional advantage is the environmental shielding that encapsulation provides for emitters.

We present a novel elastomer ridge waveguide together with a new technique to integrate a 2D heterostructure (WS<sub>2</sub>-hBN) in the mode-center of the waveguide (Figure 1a). The broadband, single-mode device supports propagation distances of several thousand micrometers and displays markedly enhanced emitter-mode coupling compared to the previous elastomer platform.<sup>[29]</sup> The enhancement relies on two factors. First, the newly developed system employs two (commercially available) polymer formulations that increase the index contrast by two orders of magnitude ( $n_1 - n_2 \approx 0.1$ ). As a result, the platform can be miniaturized, reducing the effective mode area by a factor of  $\approx 20$  from  $166.4 \mu\text{m}^2$  for the previous platform down to  $8.5 \mu\text{m}^2$ . This concentration of the electromagnetic field facilitates interaction between integrated material and guided mode, while simultaneously increasing the waveguide's collection efficiency. Second, a new fabrication sequence allows for placement of a 2D material in the mode center. This stands in contrast to a previous method where a 2D material could only be integrated off-center, that is, between the high- and low-index polymer. Therefore, emission from integrated 2D materials which arises from in-plane dipole sources couples more effectively to the

guided mode in the presented device.<sup>[35]</sup> Numerical simulations (FDTD, Lumerical) indicate that this miniaturization and optimized placement lead to an improvement of the mode overlap compared to the previous system, and that mode-center placement causes an improvement by a factor of 20 compared to off-center placement in the new platform (Figure 1b, c). This position serves as a benchmark, as it would be the most strongly coupling configuration realizable without the introduced fabrication method. We provide an experimental comparison between mode-center and off-center placement and confirm the improved interaction between mode and 2D material via collection of top-down-excited (free-space-excited) photoluminescence from the guided mode (edge-collection). This collection enables new experimental configurations and evidences significant enhancement compared to the previous platform where no signal was observable via edge-collection.

## 2. Results and Discussion

### 2.1. Coupling of Excitonic Photoluminescence to the Waveguide

To characterize optical material-waveguide coupling in the device, we employed finite-difference time-domain (FDTD) simulations and different excitation-collection schemes as outlined below. Initially, we estimated how much of the modal power flow (i.e., the Poynting vector along propagation direction) overlaps with the material for varying vertical WS<sub>2</sub> placements inside the waveguide. Modeling WS<sub>2</sub> as a 1 nm thick and 3 μm wide area perpendicular to the direction of mode propagation, we calculated a fractional power flow of 0.055% through the TMD for mode-center placement in contrast to  $6.03 \times 10^{-5}\%$  for surface placement and 0.0021% for placement below the photonic mode. This corresponds to an enhancement of the mode overlap by almost three orders of magnitude compared to surface placement and one order of magnitude compared to off-center placement.

Experimentally, we first confirmed emitter-waveguide coupling by excitation of the material from the top and collection of its photoluminescence (PL) from the guided mode via

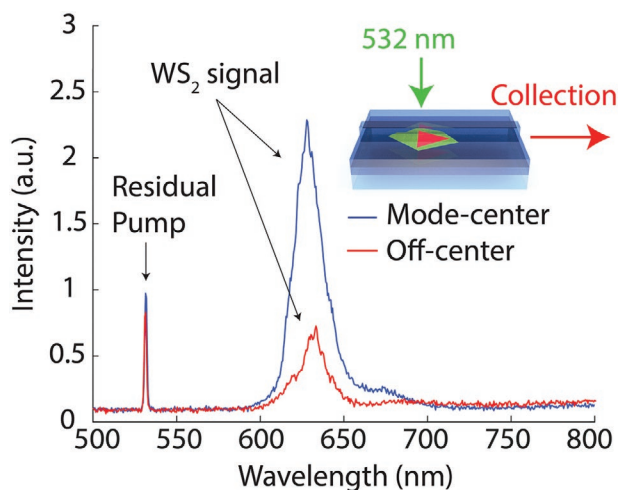


**Figure 2.** Edge-collected WS<sub>2</sub> photoluminescence from the guided mode in the developed waveguide system. The stronger WS<sub>2</sub> photoluminescence coupled to the waveguide via mode-center placement (blue) indicates its superior mode-coupling compared to off-center placement (red) (integration time = 30 s, 350 μW pump).

edge-collection (Figure 2). The detection of excitonic PL here is an important illustration of the device's improved material-waveguide coupling since the previous system did not show a signal in this configuration.<sup>[29]</sup> In these experiments, we moved the excitation spot along the waveguide-region covered by WS<sub>2</sub> and recorded the edge-collected PL for two different devices that realize either mode-center placement or off-center placement (with a material offset from the mode center by 1 μm).

We note that edge-collection of PL from the waveguide mode is possible for both the mode-center and the off-center device. The difference in coupling predicted to arise from the optimized mode-center placement is indeed observable as a higher average signal. In this configuration, however, a rigorous quantitative evaluation of the relative coupling efficiency is not possible due to setup limitations, and will be subject of future studies.

## 2.2. Excitation of WS<sub>2</sub> via the Waveguide

To investigate the relative performance of mode-center and off-center devices more closely, we established a second experimental configuration where excitation and collection points are interchanged such that we recorded the PL emitted into free space upon excitation by an edge-coupled pump (Figures 3 and 4). Using an excitation power of 40 μW ensures that we stay within the linear regime of WS<sub>2</sub> exciton emission. In this range, the collected PL intensity will be proportional to the excitation rate and serves as a measure of how well the waveguide mode couples to WS<sub>2</sub>. We compared the coupling for mode-center placement with that for off-center placement. To account for local variations in the material's quantum yield, we normalized the PL against the top-down excited and collected PL at every site. Further, we collected the emission every 2.1 μm along the waveguide where it is interfaced with the flake (Figure 3a). As anticipated, the mode-center device shows a markedly stronger response compared to the off-center device under the same excitation conditions (Figure 3). Moreover, we observed nearly exponential decay of the signal along the waveguide, indicating extinction of the waveguide mode. We measured an overall signal ratio of 11:1 for mode-center compared to off-center placement. This is evidence for the anticipated facilitation of coupling through mode-center placement, with simulations predicting a ≈ 20 times enhancement. The difference between simulation and experiment may be due to the dielectric properties of the 20 nm thick hBN support which were not included in the model.

## 2.3. Polarization-Dependent Excitation

To confirm that WS<sub>2</sub>-hBN maintains its structure and that the waveguide is, in fact, polarization-preserving, we recorded the PL in the same scheme but under variation of the pump polarization and at a fixed collection site (Figure 4). This yielded a polarization dependence of the PL signal, with an intensity

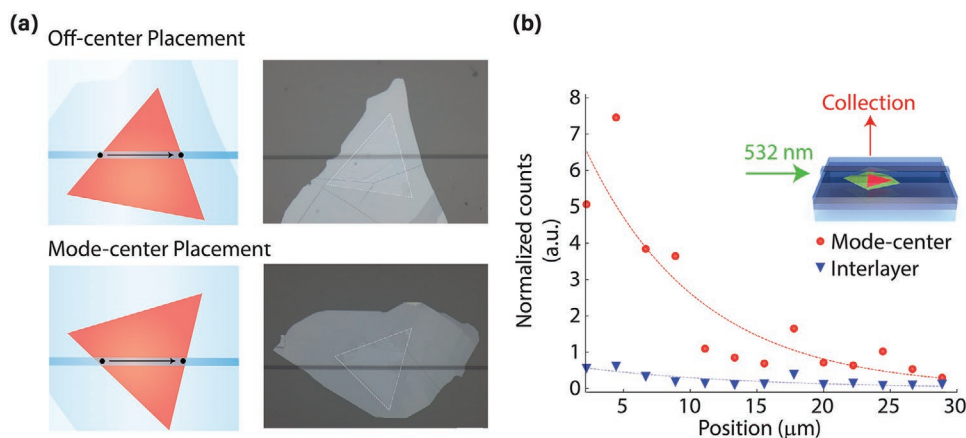


**Figure 3.** Experimental comparison of mode coupling for mode-center and off-center integrated WS<sub>2</sub>-hBN, respectively. a) The photoluminescence of WS<sub>2</sub> excited via the photonic mode is collected from free-space at different positions along the waveguide (black dots). b) Plot of the free-space collected photoluminescence at different positions normalized to account for local variations in the quantum yield. A least-square exponential fit reveals that the extinction coefficients are similar (0.08 and 0.12) and integration of the counts shows a distinctively higher excitation ratio of 11:1 for mode-center compared to off-center placement.

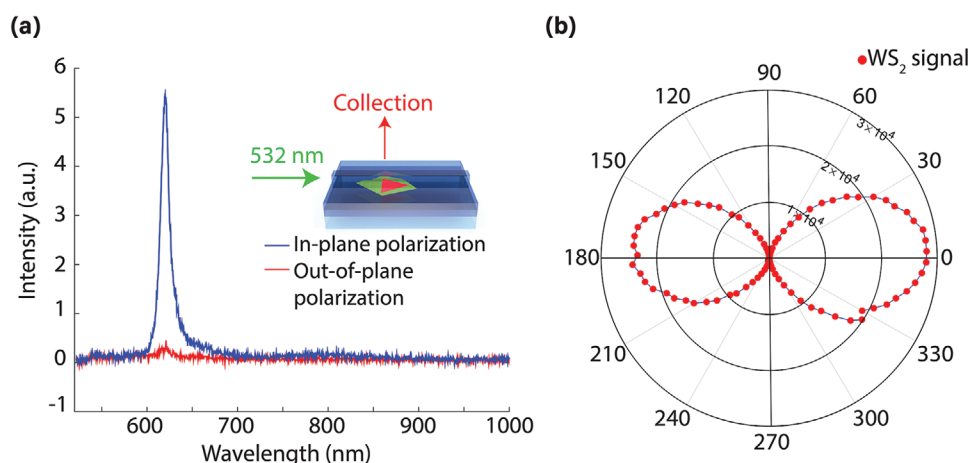


**Figure 4.** WS<sub>2</sub> photoluminescence is excited by an edge-coupled pump and measured via free-space collection. Out-of-plane polarized light shows minimal interaction with WS<sub>2</sub>. a) In-plane and out-of-plane polarized pump light couples to the waveguide and evokes photoluminescence signals with different intensities. This confirms different interaction cross-sections of pump light with the dipole-moment of 2D materials. b) A polar plot of the PL signal's integrated intensity at different pump polarizations.

that is minimal for out-of-plane-polarized pump light. The sensitivity of excitation to the pump polarization is expected due to the strictly in-plane orientation of excitons.<sup>[35]</sup> Figure 4a shows two PL spectra acquired with orthogonal pump polarizations to underline the difference in excitation ratios. The signal's dependence on pump polarization is shown in detail in a polar plot (Figure 4b), where the excitation ratio changes under gradual rotation of the pump polarization. The extinction ratio, that is, the ratio of PL intensity for in-plane and out-of-plane polarized excitation, was found to be  $\approx 65$ , indicative of this waveguide's polarization-preserving characteristics. It also serves as confirmation of the material's preserved structure throughout fabrication and transfer. A slight asymmetry in the polarization plot originates from experimental imperfections, that is, from a gradual change in alignment of the edge-coupled pump.

Weaker coupling of dipole radiation to the waveguide compared to this free-space-collected emission is expected for an in-plane oriented dipole with a Poynting vector whose angular distribution largely consists of out-of-plane components. The radiation pattern shows little overlap with the waveguide mode, producing a weaker signal compared to that collected as free-space radiation.

### 3. Conclusion

We have demonstrated a new elastomeric hybrid photonic platform where light-matter interaction with a 2D heterostructure is facilitated by miniaturization of the waveguide and mode-center integration of the material. Simulations and experiments confirm that the system exhibits significantly enhanced interaction between the encapsulated material and waveguide compared to a previous platform. The dry-transfer technique used for integration is applicable to other 2D material systems. Of note, the new devices show the ability to couple photoluminescence from the integrated materials into the waveguide mode. In addition, flexible photonic components that rely on curved

waveguides become accessible to platforms that are based on the utilized polymers.

While semiconductor platforms such as silicon-nitride waveguides can offer higher coupling efficiencies of  $\approx 7\%$  due to a higher index-contrast ( $n_{\text{Si}_3\text{N}_4} = 2.055$ ,  $n_{\text{SiO}_2} = 1.461$  at 532 nm) and a smaller mode area (of  $\approx 0.14\text{--}0.2 \mu\text{m}^2$ ),<sup>[24,36,37]</sup> the presented polymer platform offers unique features such as strain-tunability, low fabrication costs, a short development time, and a simple fabrication procedure. Mild curing conditions also enable versatile approaches to material integration. Besides fundamental studies of TMDs, and other 2D materials, we believe that this system will be of interest in the context of microfluidics, chemical-tuning, flexible photonics, optoelectronic devices, and encapsulation of other nano- and micro-scale materials into polymeric waveguides for novel hybrid systems. Last, the newly demonstrated ability to couple photoluminescence to the waveguide facilitates applications where 2D materials may also be used as integrated (non)linear and (nonclassical) light sources in the near-room-temperature regime.

### 4. Experimental Section

**Waveguide Characterization and Optical Setup:** The developed polymer platform is a ridge waveguide based on two polymers ( $n_1 \approx 1.42$  and  $n_2 \approx 1.51$  at 532 nm). Integration into the mode-center was achieved via dry-transfer of a WS<sub>2</sub>-hBN heterostructure onto a waveguide precursor and subsequent plasma-bonding of two pre-cured polymer layers that make up the lower and the upper half of the high-refractive-index layer. Each half of this guiding layer is about 1  $\mu\text{m}$  thick and the waveguide ridge has a width of 2  $\mu\text{m}$  with a height of 1  $\mu\text{m}$  (Figure 1a). The structure is capable of single-mode guiding orthogonal polarizations equally (Figure 5, top right). The refractive index difference between guiding polymer layer and the supporting polymer matrix lies between 0.085 and 0.1 and is stable over a range of wavelengths and temperatures as measured by a critical angle refractometry (Schmidt&Hänsch, see Supporting Information).<sup>[38,39]</sup>

A schematic of the experimental setup configured for an edge-coupled pump (edge-excitation) is shown in Figure 5. The polymer substrate was  $\approx 1.3 \text{ cm}$  in length and the WS<sub>2</sub>-hBN heterostructure placed



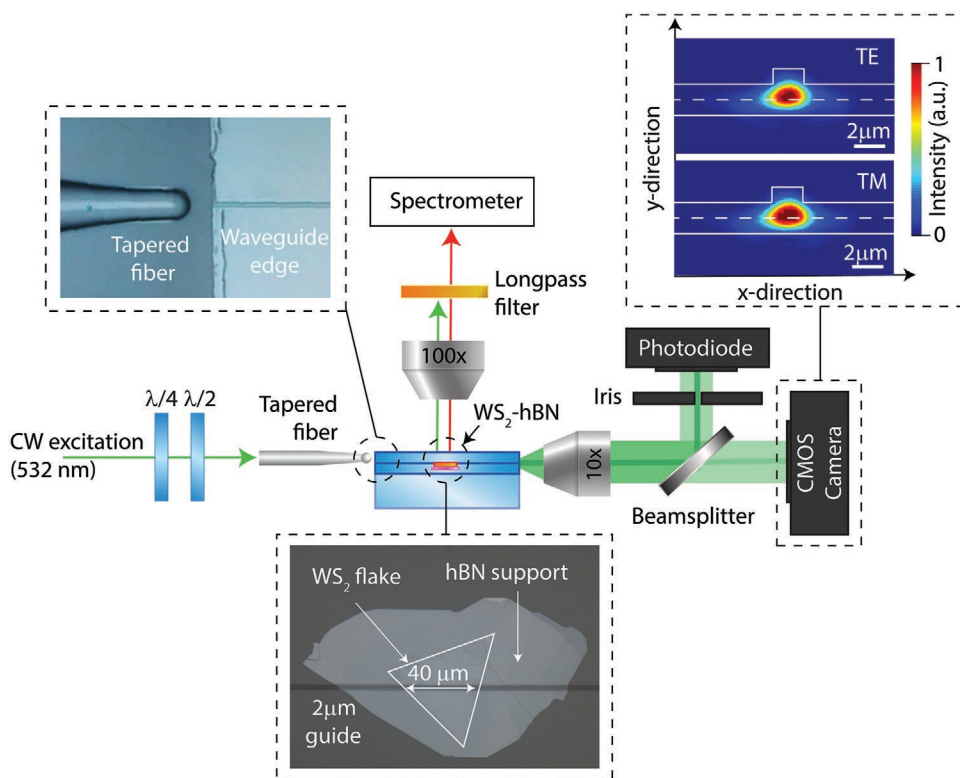


**Figure 5.** Schematic of the experimental setup configured for edge-excitation with a 532 nm pump laser and free-space collection of photoluminescence. Top left: Microscope image of a tapered fiber aligned to the waveguide for edge-coupling. Top right: Recorded images of the waveguide's output profile for orthogonal pump polarizations. White lines schematically outline the waveguide. Bottom: Microscope image of the  $WS_2$ -hBN heterostructure within the waveguide.  $WS_2$  is contained within the white lines.

close to the center of the device. Here, hBN with a thickness of 20 nm served as structural support to prevent wrinkling. The  $WS_2$  monolayer covered a length of 40  $\mu\text{m}$  along the waveguide. Fiber, waveguide and collection optics were each mounted onto three- and five-axis translation stages (ULTRAlign, Newport) for alignment. A lensed single-mode fiber (SM-630-HP, conical taper: 1.6–2  $\mu\text{m}$ ) was edge-coupled on one side and either connected to a spectrometer (NTegra system by NT-MTD) or to a 532 nm pump. A 100 $\times$  microscope objective (Olympus, 0.6 NA) was focused onto  $WS_2$  from the top and connected to either a spectrometer or a 532 nm light source. The polarization of the edge-coupled fiber was linearized using a polarizer, half-wave plate, and quarter-wave plate, with the latter precompensating for birefringence in the fiber. The edge of the waveguide chip was imaged onto a CMOS camera using a 10 $\times$  objective lens to facilitate and monitor fiber alignment. An additional nonpolarizing beam splitter in this optical collection path allowed for simultaneous monitoring of both the transmitted output profile and the transmitted power via a power meter. An iris ensured that only the guided mode's intensity evolution was recorded. All experiments were performed at room-temperature. A detailed characterization of the heterostructure before and after transfer can be found in the Supporting Information.

**Waveguide Fabrication:** The waveguides were fabricated from two different PDMS formulations (Sylgard 184 (Dow Corning) and Gelest OE 50 (Mitsubishi Chemicals)) on two silicon wafers. To create the waveguide ridge with mode-center placement, a silicon wafer was spin-coated with a 1  $\mu\text{m}$  thick layer of positive photoresist (AZ1512). The waveguide pattern was laser-written into this layer. Gelest OE 50 was spin-coated onto this mold to a thickness of  $\approx 1$   $\mu\text{m}$ . The wafer was cured at 55  $^\circ\text{C}$  for 4 h and the TMD-hBN heterostructure transferred via soft lithography, making up the first half of the guiding layer. A second, unpatterned and photoresist-coated substrate was prepared again by spin-coating and curing of a 1  $\mu\text{m}$  thick layer of Gelest OE 50 on the AZ-coated wafer. A 2 mm thick layer of Sylgard 184 (the lower-refractive

index polymer) was cured on top of this second substrate at 70  $^\circ\text{C}$  for 1 h. This substrate now contained the lower part of the guiding layer (Gelest OE 50) and its support matrix (Sylgard 184). After treatment with oxygen plasma for 30 s, the two halves were brought in contact, forming a permanent bond and completing the structure. For off-center placement, the thickness of the high-index polymer-layer was increased to 2  $\mu\text{m}$ ,  $WS_2$ -hBN with the same dimensions as for the mode-center device was transferred onto it and the layer was plasma bonded directly to the low-index polymer.

**Material Transfer:** The  $WS_2$ -hBN heterostructure was assembled using a pick-up technique.  $WS_2$  monolayers were first grown onto Si substrates via a liquid-mediated chemical vapor deposition method. hBN flakes were tape-exfoliated from bulk hBN crystals supplied by the National Institute for Materials Science (NIMS), Japan, onto polydimethylsiloxane (PDMS) substrates (Sylgard 184). These hBN flakes were subsequently used to pick up the CVD-grown  $WS_2$  flakes. During the pick-up, the  $WS_2$  samples were heated to 130  $^\circ\text{C}$  to facilitate the pick-up process. Last, the  $WS_2$ -hBN heterostack was released onto the waveguide using a dry-transfer technique.

## Supporting Information

Supporting Information is available from the Wiley Online Library or from the author.

## Acknowledgements

A.L. acknowledges support by the National Research Foundation, Prime Minister's Office, Singapore. G.E. acknowledges support

from the Ministry of Education (MOE), Singapore, under AcRF Tier 3 (MOE2018-T3-1-005) and the Singapore National Research Foundation for funding the research under the medium-sized center program. M.S. acknowledges funding from the European Research Council (PoC 3DprintedOptics, grant 862549), Bundesministerium für Bildung und Forschung (Printoptics), Baden-Wuerttemberg Stiftung (Opterial), DFG GRK 2642, and MWK ICM. J. V.-G. gratefully acknowledges financial support from the Portuguese Foundation for Science and Technology (FCT), Portugal 2020 and Compete2020 through the project PTDC/NAN-OPT/29265/2017. The authors thank Prof. Harald Giessen for the helpful correspondence and for facilitating material characterization and thank Isa Ahmadi for fruitful discussions.

## Conflict of Interest

The authors declare no conflict of interest.

## Data Availability Statement

The data that support the findings of this study are available from the corresponding author upon reasonable request.

## Keywords

2D materials, flexible photonics, hybrid photonics, photonic integrated circuits, transition metal dichalcogenides, waveguides

Received: August 13, 2021

Revised: October 11, 2021

Published online: November 6, 2021

- [1] L. M. Malard, T. V. Alencar, A. P. M. Barboza, K. F. Mak, A. M. de Paula, *Phys. Rev. B* **2013**, *87*, 201401.
- [2] X. Yin, Z. Ye, D. A. Chenet, Y. Ye, K. O'Brien, J. C. Hone, X. Zhang, *Science* **2014**, *344*, 488.
- [3] K. F. Mak, J. Shan, *Nat. Photonics* **2016**, *10*, 216.
- [4] Z. Sun, A. Martinez, F. Wang, *Nat. Photonics* **2016**, *10*, 227.
- [5] A. Srivastava, M. Sidler, A. V. Allain, D. S. Lembke, A. Kis, A. Imamoglu, *Nat. Nanotechnol.* **2015**, *10*, 491.
- [6] M. Koperski, K. Nogajewski, A. Arora, V. Cherkez, P. Mallet, J.-Y. Veuillen, J. Marcus, P. Kossacki, M. Potemski, *Nat. Nanotechnol.* **2015**, *10*, 503.
- [7] T. T. Tran, S. Choi, J. A. Scott, Z.-Q. Xu, C. Zheng, G. Seniutinas, A. Bendavid, M. S. Fuhrer, M. Toth, I. Aharonovich, *Adv. Opt. Mater.* **2017**, *5*, 1600939.
- [8] T. Chu, H. Ilatikhameneh, G. Klimeck, R. Rahman, Z. Chen, *Nano Lett.* **2015**, *15*, 8000.
- [9] Q. H. Wang, K. Kalantar-Zadeh, A. Kis, J. N. Coleman, M. S. Strano, *Nat. Nanotechnol.* **2012**, *7*, 699.
- [10] P. Rivera, H. Yu, K. L. Seyler, N. P. Wilson, W. Yao, X. Xu, *Nat. Nanotechnol.* **2018**, *13*, 1004.
- [11] S. Mouri, Y. Miyauchi, K. Matsuda, *Nano Lett.* **2013**, *13*, 5944.
- [12] A. Castellanos-Gomez, R. Roldán, E. Cappelluti, M. Buscema, F. Guinea, H. S. J. van der Zant, G. A. Steele, *Nano Lett.* **2013**, *13*, 5361.
- [13] A. W. Elshaari, W. Pernice, K. Srinivasan, O. Benson, V. Zwiller, *Nat. Photonics* **2020**, *14*, 285.
- [14] P. Sibson, C. Erven, M. Godfrey, S. Miki, T. Yamashita, M. Fujiwara, M. Sasaki, H. Terai, M. G. Tanner, C. M. Natarajan, R. H. Hadfield, J. L. O'Brien, M. G. Thompson, *Nat. Commun.* **2017**, *8*, 13984.
- [15] F. Flamini, N. Spagnolo, F. Sciarrino, *Rep. Prog. Phys.* **2018**, *82*, 016001.
- [16] M. Chamanzar, Z. Xia, S. Yegnanarayanan, A. Adibi, *Opt. Express* **2013**, *21*, 32086.
- [17] D. Kohler, G. Schindler, L. Hahn, J. Milvich, A. Hofmann, K. Länge, W. Freude, C. Koos, *Light: Sci. Appl.* **2021**, *10*, 64.
- [18] M. A. G. Porcel, A. Hinojosa, H. Jans, A. Stassen, J. Goyvaerts, D. Geuzebroek, M. Geiselmann, C. Dominguez, I. Artundo, *Opt. Laser Technol.* **2019**, *112*, 299.
- [19] P. Tonndorf, O. Del Pozo-Zamudio, N. Gruhler, J. Kern, R. Schmidt, A. I. Dmitriev, A. P. Bakhtinov, A. I. Tartakovskii, W. Pernice, S. Michaelis de Vasconcellos, R. Bratschitsch, *Nano Lett.* **2017**, *17*, 5446.
- [20] S. Joshi, B. K. Kaushik, *Nanotechnology* **2020**, *31*, 435202.
- [21] G. Q. Ngo, A. George, R. T. K. Schock, A. Tuniz, E. Najafidehaghani, Z. Gan, N. C. Geib, T. Bucher, H. Knopf, S. Saravi, C. Neumann, T. Lühder, E. P. Schartner, S. C. Warren-Smith, H. Ebendorff-Heidepriem, T. Pertsch, M. A. Schmidt, A. Turchanin, F. Eilenberger, *Adv. Mater.* **2020**, *32*, 2003826.
- [22] Y. Zuo, W. Yu, C. Liu, X. Cheng, R. Qiao, J. Liang, X. Zhou, J. Wang, M. Wu, Y. Zhao, P. Gao, S. Wu, Z. Sun, K. Liu, X. Bai, Z. Liu, *Nat. Nanotechnol.* **2020**, *15*, 987.
- [23] T. Vogl, Y. Lu, P. K. Lam, *J. Phys. D: Appl. Phys.* **2017**, *50*, 295101.
- [24] F. Peyskens, C. Chakraborty, M. Muneeb, D. Van Thourhout, D. Englund, *Nat. Commun.* **2019**, *10*, 4435.
- [25] J. He, I. Paradisanos, T. Liu, A. R. Cadore, J. Liu, M. Churayev, R. N. Wang, A. S. Raja, C. Javerzac-Galy, P. Roelli, D. D. Fazio, B. L. T. Rosa, S. Tongay, G. Soavi, A. C. Ferrari, T. J. Kippenberg, *Nano Lett.* **2021**, *21*, 2709.
- [26] O. Iff, D. Tedeschi, J. Martín-Sánchez, M. Moczala-Dusanowska, S. Tongay, K. Yumigeta, J. Taboada-Gutiérrez, M. Savaresi, A. Rastelli, P. Alonso-González, S. Höfling, R. Trotta, C. Schneider, *Nano Lett.* **2019**, *19*, 6931.
- [27] C. Errando-Herranz, E. Schöll, R. Picard, M. Laini, S. Cyger, A. W. Elshaari, A. Branny, U. Wennberg, S. Barbat, T. Renaud, M. Sartison, M. Brotons-Gisbert, C. Bonato, B. D. Gerardot, V. Zwiller, K. D. Jöns, *ACS Photonics* **2021**, *8*, 1069.
- [28] J.-H. Kim, S. Aghaeimeibodi, J. Carolan, D. Englund, E. Waks, *Optica* **2020**, *7*, 291.
- [29] F. Aukstolz, D. Vella, I. Verzhbitskiy, K. F. Ng, Y. W. Ho, J. A. Grieve, J. Viana-Gomes, G. Eda, A. Ling, *ACS Photonics* **2019**, *6*, 595.
- [30] D. Pérez-Calixto, D. Zamarrón-Hernández, A. Cruz-Ramírez, M. Hautefeuille, J. Hernández-Cordero, V. Velázquez, M. Grether, *Opt. Mater. Express* **2017**, *7*, 1343.
- [31] S. Shabahang, F. Clouser, F. Shabahang, S.-H. Yun, *Adv. Opt. Mater.* **2021**, *9*, 2100270.
- [32] J. S. Kee, D. P. Poenar, P. Neuzil, L. Yobas, *Opt. Express* **2009**, *17*, 11739.
- [33] J. Missinne, S. Kalathimekkad, B. V. Hoe, E. Bosman, J. Vanfleteren, G. V. Steenberge, *Opt. Express* **2014**, *22*, 4168.
- [34] J. A. Grieve, K. F. Ng, M. J. L. F. Rodrigues, J. Viana-Gomes, A. Ling, *Appl. Phys. Lett.* **2017**, *111*, 211106.
- [35] J. A. Schuller, S. Karaveli, T. Schiros, K. He, S. Yang, I. Kymissis, J. Shan, R. Zia, *Nat. Nanotechnol.* **2013**, *8*, 271.
- [36] K. Luke, Y. Okawachi, M. R. E. Lamont, A. L. Gaeta, M. Lipson, *Opt. Lett.* **2015**, *40*, 4823.
- [37] I. H. Malitson, *J. Opt. Soc. Am.* **1965**, *55*, 1205.
- [38] T. Gissibl, S. Wagner, J. Sjkora, M. Schmid, H. Giessen, *Opt. Mater. Express* **2017**, *7*, 2293.
- [39] M. Schmid, D. Ludescher, H. Giessen, *Opt. Mater. Express* **2019**, *9*, 4564.